AUT Journal of Mechanical Engineering

AUT J. Mech. Eng., 6(4) (2022) 561-578
DOI: 10.22060/ajme.2022.20917.6025

Transient Response of Laminated Composite Curved Beams with General Boundary Conditions under Moving Force

A. Ahmadi, M. Abedi*

Department of Mechanical Engineering, University of Mazandaran, Babolsar, Iran.

ABSTRACT: Vibrational analysis of beams has been an important subject for many years. Despite the wide applications of curved beams, especially laminated composite curved beams, less attention has been paid to this subject. In this study, the transient response of the laminated composite curved beam due to a moving force with constant velocity for different boundary conditions has been obtained. By employing Hamilton's principle, the equations of motion along with the corresponding boundary conditions of the beam are determined. The finite element method is employed to solve these equations. Using the eigenvalue technique, the vibrational characteristics of the beam are calculated. Results for the free and forced vibration of the beam have been compared against available data in the literature and the three-dimensional model in ANSYS. The effects of different parameters such as the geometry of the beam, fibers orientation, and boundary conditions on the transient response of the beam have been investigated. It has been shown that beam with cross-ply layups has lower values of transient deflection compared to the angle-ply layups. Also, the anti-symmetric cross-ply beam has more deflection with respect to the symmetric one.

Review History:

Received: Nov. 24, 2021

Revised: May, 21, 2022

Accepted: Aug. 21, 2022

Available Online: Aug. 29, 2022

Keywords:

Curved beam

Moving force

Laminated composite beam.

1- Introduction

The dynamic response of structures under moving loads is crucial during their operation life. Elements in structures are known to be a bar, rods, columns, or beams which can be recognized by their loading conditions. Beam's application in industries such as aerospace, submarine, automotive, and the construction of many structures in civil and mechanical engineering is not hidden from anyone. For example, bridge structures, rotating shafts, robotic arms, and space vehicles are usually modeled by beams subjected to static and dynamic loads. It is obvious that a beam experience greater deflections and stresses under dynamic loads in comparison to static loads, and these differences motivated numerous researchers to focus on the forced vibration of beams in past decades [1-5].

In recent years, composite materials with their specific behavior such as lightweight, corrosion resistant, high strength, and stiffness have been used in many engineering structures, and their dynamic response under moving loads became an interesting field for civil and mechanical engineers. Kiral et al. [6] studied the dynamic behavior of laminated composite beams subjected to a single force with constant velocity. The Finite Element Method (FEM) based on classical lamination theory was used in this article and the results were compared against the isotropic simple beam. Kahya [7] proposed an approach for vibration analysis of the intact laminated composite beam based on the shear deformation theory. It was concluded that angle-ply laminated beams are more sensitive to moving loads. Kargarnovin et al. [8] investigated the results of the delaminated Timoshenko beam under the action of moving load by considering Poisson's effect, shear deformation, and rotary inertia. Galerkin's method was used to obtain the transient response. It was concluded that the existence of any single delamination can increase the dynamic deflection of the beam. Kadivar and Mohebpour [9] compared the dynamic response of laminated composite beams with different layups and subjected to moving force. By expressing lateral strains and curvatures in terms of the axial, transverse strains and curvatures, the effect of couplings was considered. Classical Lamination Theory (CLT), First-order Shear Deformation Theory (FSDT), and Higher-order Shear Deformation Theory (HSDT) were used to obtain the transient response. Jafari-Talookolaei et al. [10] studied the dynamic response of delaminated composite beams using the finite element method. Dynamic analysis of composite sandwich beams under the action of a moving mass was investigated by Kahya and Mosallam [11]. Zibdeh and Abu-Hilal [12] analyzed the stochastic vibrations of a laminated composite-coated intact beam traversed by a random moving load.

While forced vibration of straight beams has been the subject of numerous studies [6-12], composite curved beams in spite of their practical applications such as curved bridges, elevated railroads, and aerospace applications have been

*Corresponding author's email: m.abedi@umz.ac.ir

less likely analyzed during the past decades. Genin et al. [13] used a general algorithm for the moving mass problem and developed it to analyze the curved bridge response due to the moving mass. For this purpose, Green functions were applied to derive two coupled integral-differential equations of curved bridges. Differential equations were transferred into the matrix form to derive the response of the bridges. By considering only the first mode of vibration, Yang et al. [14] derived an analytical solution for forced vibration analysis of the single-layer curved beam. The accuracy of the results was validated with numerical solutions. Wu and Chiang [15] studied the forced vibration of the Timoshenko curved beam. It has been shown that utilizing a local polar coordinate system instead of the local Cartesian system for the element property matrices can reduce calculations during solution processes. Curved beams subjected to three directional moving loads were studied by Li and Ren [16]. Vertical, torsional, radial, and axial vibrations were considered using Galerkin's method along with the modal superposition method. In the above-mentioned studies, a single-layer beam was considered. Likewise, in many studies, only the first mode has been considered while it is clear that higher modes play an important role in the transient response of the beam. Arefi and Zenkour [17] presented the transient formulation for a three-layer curved nanobeam in thermo–magneto-elastic environments. The curved nanobeam included a nanocore and two integrated piezo-magnetic layers subjected to electric and magnetic potentials and transverse loads resting on a Pasternak foundation. In another work, Arefi et al. [18] used the principle of virtual work to obtain the equations for functionally graded curved nanobeam reinforced with nanoplatelets. Hajianmaleki and Qatu [19] developed a new equivalent modulus of elasticity for a laminated composite curved beam. In addition, they also represented equivalent stiffness parameters for curved beams to consider the effect of all couplings. In another study by Ye et al. [20], free vibration analysis of laminated deep curved beam with arbitrary boundary condition was studied. To derive the equations of motion and boundary conditions, Hamilton's principle was employed and a series solution was used to solve these equations. A parametric study was represented in order to show the effects of shear deformation, inertia rotary, and deepness term. Jafari-Talookolaei et al. [21] studied the free vibrations of laminated composite curved beams with single delamination. Having continuity conditions at the delamination boundaries and using Hamilton's principle, equilibrium conditions were derived. To solve the equations of motions, analytical and finite element solutions were applied. Parametric studies were done to show the effects of delamination size and locations, layups configurations, boundary conditions and material anisotropy on the dynamic responses. It was observed that the delamination reduces the natural frequencies. Qin et al. [22] proposed analytical solution for curved composite I-beam and compared results against FEM. They concluded that by increasing the shear connector's stiffness, the beam seems more likely to be a rigid structure. Luo et al. [23] studied Euler-Bernoulli curved beam by Galerkin' method using sinusoidal Fourier series, and by extending the approach, they investigated the train-track spatial interaction.

Shao et al. [24] obtained the dynamic response of composite laminated curved beams with arbitrary lamination schemes and general boundary constraints by the method of reverberation ray matrix. To consider general boundary conditions, two pairs of linear springs and one pair of rotational springs were employed at the end of the beam. The exact solution for the transient response of a curved beam under unit transverse impact force was proposed by exerting Neumann series expansion and the fast Fourier transform algorithm. In another work by Kurtaran [25], the transient response of laminated composite curved beam under the tip load and uniformly distributed load has been studied. FSDT was used and the Generalized Differential Quadrature (GDQ) method was employed to derive the results. It has been observed that the GDQ method with FEM provides good accuracy for the transient analysis of laminated composite curved beams. Zhao et al. [26] studied a carbon fiber-reinforced composite circular arch with porous graphene platelet coating in a hydrothermal environment with general boundary conditions. Verification of results was carried out by comparing results with available literature. Subsequently, a forced response that can be divided into steady-state response and transient response has been computed. It should be mentioned that transient response was conducted for four different pulse functions to consider the impact resistance of the arch. Sarparast and Ebrahimi-Mamaghani [27] presented a new analysis of composite laminated curved beams under a moving load and sequences of moving loads. They, however, proposed expressions for calculating resonance, maximum resonance, resonance disappearance, and two types of cancellation. Moreover, the cancellation phenomenon of laminated curved beams under moving loads has been studied. It has to be mentioned that in this paper, only the first mode of vibration for simply supported beam has been considered.

In the present paper, a laminated composite curved beam under the action of moving radial force has been studied. Considering the first mode of vibration to analyze the beam does not provide accurate results. Due to this fact, a laminated composite curved beam with general boundary conditions and subjected to the moving load is studied by considering higher modes of vibration. The finite element method has been used to calculate the natural frequencies, mode shapes, and dynamic response of the laminated curved beam. It is worth mentioning that by assuming an artificial spring at the ends of the beam, we are capable of setting the stiffness of springs to model different boundary conditions. Choosing a suitable number of elements in FEM enables us to calculate the natural frequencies and mode shapes accurately in our one-dimensional model in comparison with 3D analysis in ANSYS.

This study is organized as follows. First, the mathematical model of the beam and its equations of motion are given. Then, the solution procedure has been presented in the next section. Subsequently, by using the eigenvalue technique,

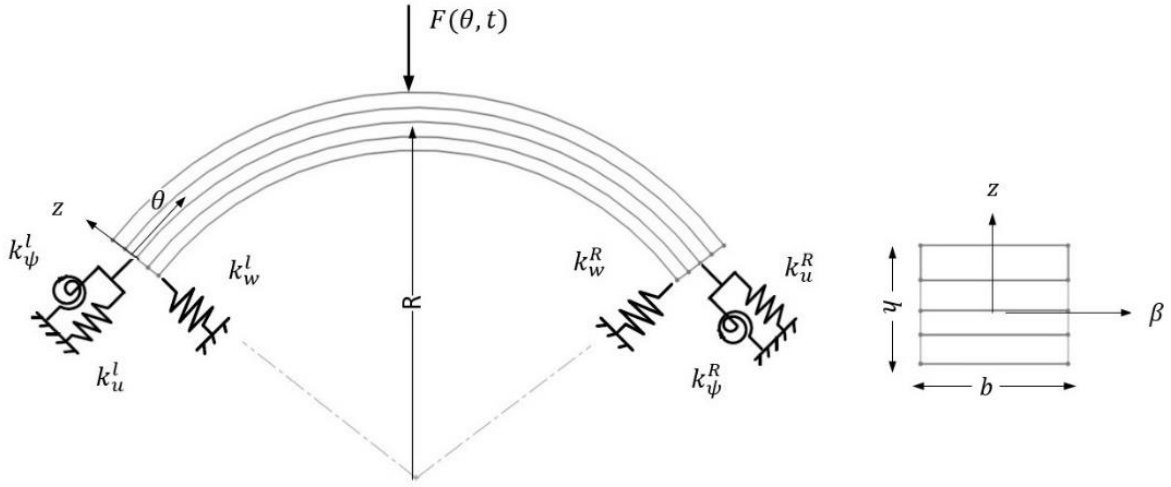

Fig. 1. Schematic view of the laminated curved beams

frequencies and mode shapes of the beam are obtained and results are compared against available results in literature and ANSYS. To further validate the present model, the forced vibration of the beam is compared with ANSYS. The parametric study is employed to investigate the effect of different parameters such as boundary condition, total angle of the curved beam, and fiber orientation on the response. In the end, the conclusions of this study are represented.

2- Governing Equations of Motion

Schematic view of the considered laminated composite curved beam is shown in Fig. 1. As it can be seen the laminated curved beam consists of N orthotropic laminas. Arbitrary boundary conditions are considered by assuming artificial springs at both ends of the beam. It is assumed that the beam has a constant thickness h and the thickness of each lamina can be calculated as $(h_i = \frac{h}{N})$.

The radius of the beam from the middle surface is R, and its angle and width are θ_0 and b, respectively. The coordinates θ, β and z are taken along the beam's length, width, and thickness direction, respectively.

In order to consider the effects of shear deformation and rotary inertia, first-order shear deformation theory is employed. So, the generalized displacements can be expressed as:

$$\begin{aligned} u &= u_0 + z\psi \\ w &= w_0 \end{aligned} \tag{1}$$

In which u and w indicate displacements along the θ and z directions, respectively. Likewise, u_0 and w_0 represent the displacements of the middle surface and ψ is the bending rotation. Normal strain, ε_θ, curvature, χ_θ, and shear strain, $\gamma_{\theta z}$ of the beam can be calculated as follows:

$$\varepsilon_\theta = \frac{\partial u}{R\partial\theta} + \frac{w}{R} \tag{2}$$

$$\chi_\theta = \frac{\partial \psi}{R\partial\theta} \tag{3}$$

$$\gamma_{\theta Z} = \frac{\partial w}{R\partial\theta} - \frac{u}{R} + \psi \tag{4}$$

Based on FSDT, the force and moment resultants are defined as [21]:

$$\begin{Bmatrix} N_\theta \\ M_\theta \\ Q_\theta \end{Bmatrix} = \begin{bmatrix} A_{11} & B_{11} & 0 \\ B_{11} & D_{11} & 0 \\ 0 & 0 & A_{55} \end{bmatrix} \begin{Bmatrix} \varepsilon_\theta \\ \chi_\theta \\ \gamma_{\theta Z} \end{Bmatrix} \tag{5}$$

Where $N_\theta, M_\theta, Q_\theta$ are the in-plane force, bending moment, and shear force, respectively. It has to be mentioned that A_{11}, B_{11} and D_{11} are the extensional, bending-extension coupling and bending stiffnesses, and A_{55} is the shear stiffness. These coefficients are obtained as:

$$A_{11} = Rb\sum_{k=1}^{N} E_{xk} \ln(\frac{R+z_{k+1}}{R+z_k}) \quad (6)$$

$$B_{11} = Rb\sum_{k=1}^{N} E_{xk}[(z_{k+1}-z_k) - R\ln(\frac{R+z_{k+1}}{R+z_k})] \quad (7)$$

$$A_{55} = K_s b\sum_{k=1}^{N} Q_{55k}[(z_{k+1}-z_k) - \frac{4}{3h^2}\{(z_{k+1})^3 - (z_k)^3\}] \quad (8)$$

$$D_{11} = Rb\sum_{k=1}^{N} E_{xk}[\frac{(R+z_{k+1})^2-(R+z_k)^2}{2} - 2R(z_{k+1}-z_k) + R^2\ln(\frac{R+z_{k+1}}{R+z_k})] \quad (9)$$

In which z_{k+1} and z_k are the distances from the laminate midplane to the top and bottom of the k^{th} layer, respectively. Likewise, K_s stands for shear correction factor. For the beam with a rectangular cross-section, this factor is $K_s = \frac{5}{6}$ [21]. In addition, E_{xk} indicates the equivalent modulus of elasticity and Q_{55k} is the transformed shear stiffness of each lamina and are obtained from the following equations [21]:

$$\frac{1}{E_{xk}} = \frac{\cos^4(\theta_k)}{E_{11k}} + (\frac{1}{G_{12k}} - \frac{2\nu_{12k}}{E_{11k}})\cos^2(\theta_k)\sin^2(\theta_k) + \frac{\sin^4(\theta_k)}{E_{22k}} \quad (10)$$

$$Q_{55k} = G_{13k}\cos^2(\theta_k) + G_{23k}\sin^2(\theta_k) \quad (11)$$

Where E_{11} is the elastic modulus of the composite material along the direction parallel to the fiber. Moreover, E_{22} is the elastic modulus along the direction perpendicular to the fiber and G_{ij} is the shear modulus in the i-j plane. ν_{12}, ν_{21} are the Poisson's ratios and θ_k is the angle of the fiber orientation of each layer [25].

Beam's equations of motion are derived by employing Hamilton's principle:

$$\int_{t_2}^{t_2} \delta^{(1)}(T + W_F - U)dt = 0 \quad (12)$$

In which T, w_F and U denote the kinetic energy, work done by moving load, and potential energy, respectively. Moreover, $\delta^{(1)}$ denotes the first variation of the functional. Potential energy is divided into two parts: the potential energy of the beam, U_B, and the potential energy of the boundary springs, U_{AS}. These terms are calculated as follows:

$$U_B = \frac{1}{2}\int_0^{\theta_0} (N_\theta \varepsilon_\theta + M_\theta \chi_\theta + Q_\theta \gamma_{\theta z}) R d\theta \quad (13)$$

$$U_{AS} = \frac{1}{2}[K_u^l u^2 + K_w^l w^2 + K_\psi^l \psi^2]_{\theta=0} + \frac{1}{2}[K_u^R u^2 + K_w^R w^2 + K_\psi^R \psi^2]_{\theta=\theta_0} \quad (14)$$

In Eq. (14), K_u^l, K_w^l, K_ψ^l are the linear and rotational springs' stiffness at the left side of the beam. Similarly, K_u^R, K_w^R, K_ψ^R are the springs' stiffness at the right side of the beam. It should be noted that by allocating different values for the springs' stiffness, different boundary conditions can be set.

By substituting the Eqs. (2) to (5) into Eq. (13), the potential energy in terms of displacement components can be written as:

$$U_B = \frac{1}{2}\int_0^{\theta_0} [A_{11}(\frac{\partial u}{R\partial\theta} + \frac{w}{R})^2 + 2B_{11}\frac{\partial \psi}{R\partial\theta}(\frac{\partial u}{R\partial\theta} + \frac{w}{R})^2 + D_{11}(\frac{\partial \psi}{R\partial\theta})^2 + A_{55}(\frac{\partial w}{R\partial\theta} - \frac{u}{R} + \psi)]R d\theta \quad (15)$$

In the second term of Eq. (12), W_F is the work done by moving load defined as [10]:

$$W_F = \int_0^{\theta} F(t)\delta(R\theta - \nu t)\, w\, R d\theta \quad (16)$$

It is assumed that radial point force $F(t)$ moves along the beam with constant velocity ν. It is worth mentioning that δ is the Dirac delta function.

Subsequently, the corresponding kinetic energy for the curved beam is obtained as [21]:

$$T = \frac{1}{2}\int_0^{\theta_0} [\overline{I_0}(\frac{\partial u}{\partial t})^2 + 2\overline{I_1}(\frac{\partial u}{\partial t})(\frac{\partial \psi}{\partial t}) + \overline{I_2}(\frac{\partial \psi}{\partial t})^2 + \overline{I_0}(\frac{\partial w}{\partial t})^2] R d\theta \quad (17)$$

In the above-mentioned equation, the inertia terms can be calculated by the following equations:

$$\overline{I_0} = I_0 + \frac{I_1}{R}$$
$$\overline{I_1} = I_1 + \frac{I_2}{R}$$
$$\overline{I_2} = I_2 + \frac{I_2}{R}$$
$$[I_0, I_1, I_2, I_3] = b\sum_{k=1}^{N}\int_{z_k}^{z_{k+1}} \rho_k[1, z, z^2, z^3]dz \quad (18)$$

By substituting Eqs. (14) to (17) into Eq. (12), differential equations of motion and the corresponding boundary conditions can be determined after some mathematical manipulations:

$$\begin{aligned}
&\frac{\partial N_\theta}{\partial\theta}-I_0R\frac{\partial^2u}{\partial t^2}+Q_\theta-I_1\frac{\partial^2\psi}{\partial t^2}=0\\
&-N_\theta+\frac{\partial Q_\theta}{\partial\theta}-I_0R\frac{\partial^2u}{\partial t^2}+F_0\delta(R\theta-vt)=0\\
&\frac{\partial M_\theta}{\partial\theta}-RQ_\theta-I_1\frac{\partial^2u}{\partial t^2}+I_2R\frac{\partial^2\psi}{\partial t^2}=0
\end{aligned}\tag{19}$$

$$\begin{aligned}
&N_\theta(\delta u_{(\theta=0)})-K_u^l u_{(\theta=0)}=0\\
&Q_\theta(\delta w_{(\theta=0)})-K_w^l\delta w_{(\theta=0)}=0\\
&M_\theta(\delta\psi_{(\theta=0)})-K_\psi^l\delta\psi_{(\theta=0)}=0
\end{aligned}\tag{20}$$

$$\begin{aligned}
&-N_\theta(\delta u_{(\theta=\theta_0)})-K_u^R u_{(\theta=\theta_0)}=0\\
&-Q_\theta(\delta w_{(\theta=\theta_0)})-K_W^R w_{(\theta=\theta_0)}=0\\
&-M_\theta(\delta\psi_{(\theta=\theta_0)})-K_\psi^R u_{(\theta=\theta_0)}=0
\end{aligned}\tag{21}$$

Where Eq. (19) denotes equations of motion and Eqs. (20) and (21) are the boundary conditions at the left and right ends of the beam, respectively. By assigning the proper value for the stiffnesses of the boundary springs, the general boundary conditions can be modeled. For instance, the free and clamped end conditions can be modeled by assuming $k=0$ and $k\to\infty$, respectively. The below stiffnesses are considered to model simple (S), clamped (C), and free (F) conditions:

$$\begin{aligned}
&S: k_u=k_w=10^7\frac{E_{11}}{12(1-\nu_{12}\nu_{21})}, k_\psi=0\\
&C: k_u=k_w=10^7\frac{E_{11}}{12(1-\nu_{12}\nu_{21})}, k_\psi=10^7\frac{E_{11}h^2}{12(1-\nu_{12}\nu_{21})}\\
&F: k_u=k_w=k_\psi=0
\end{aligned}\tag{22}$$

3- Solution

To solve differential equations of the beam, the finite element method is used. The mass and stiffness matrices of each element are calculated. We used higher order curved beam element with three nodes. Each node has three degrees of freedom, namely u, w and ψ, which shows displacement fields of the middle surface along θ, z and β axis, respectively. Fig. 2 (a) shows a typical element in which the location of nodes in the middle surface has been depicted. The intrinsic coordinate ζ is defined as $(\zeta=\frac{\theta}{\theta_0^e})$ (Fig. 2 (b)). By employing Lagrangian interpolation functions, i.e., $N_i(\zeta)$, displacement components of the beam are interpolated as follows [21]:

$$\begin{aligned}
&u=\sum_{i=1}^{3}N_i(\zeta)u_i\\
&w=\sum_{i=1}^{3}N_i(\zeta)w_i\\
&\psi=\sum_{i=1}^{3}N_i(\zeta)\psi_i
\end{aligned}\tag{23}$$

$$\begin{aligned}
&N_1=2\zeta^2-3\zeta+1\\
&N_2=4(\zeta-\zeta^2)\\
&N_3=2\zeta^2-\zeta
\end{aligned}\tag{24}$$

It should be said that in Eq. (23), (u_i, w_i, ψ_i) are the degrees of freedom of the i^{th} node. By defining $\Delta=\{u_1,w_1,\psi_1,u_2,w_2,\psi_2,u_3,w_3,\psi_3\}^T$ as the vector of degrees of freedom for the element, Eq. (23) can be rewritten in the matrix form, i.e., $u=[N_u]\Delta, w=[N_w]\Delta, \psi=[N_\psi]\Delta$ in which:

$$\begin{aligned}
&[N_u]=[N_1,0,0,N_2,0,0,N_3,0,0]\\
&[N_w]=[0,N_1,0,0,N_2,0,0,N_3,0]\\
&[N_\psi]=[0,0,N_1,0,0,N_2,0,0,N_3]
\end{aligned}\tag{25}$$

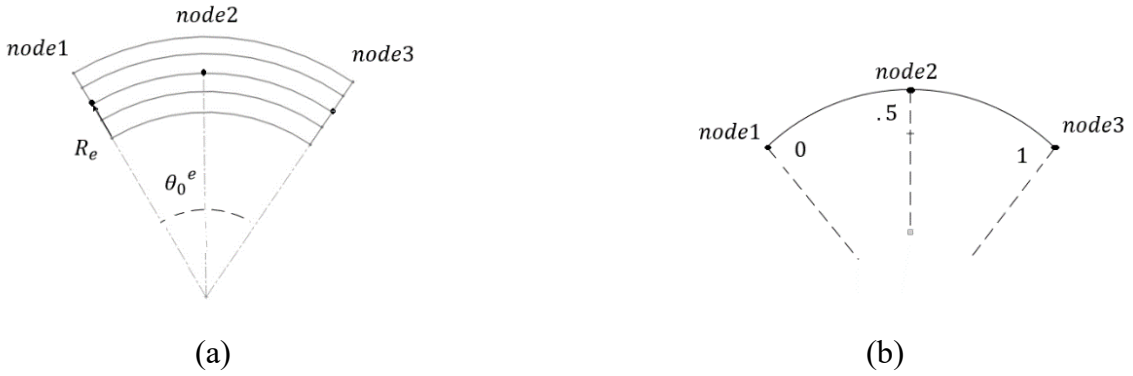

Fig. 2. (a) A higher-order curved beam element, and (b) its intrinsic coordinates [21]

Table 1. Material and geometrical properties of the curved beam [27]

$R=1\,(\mathrm{m})$	$\theta_0=\frac{2\pi}{3}\,\mathrm{rad}$	$G_{13}=5.5\,\mathrm{Gpa}$	$E_{22}=10\,\mathrm{Gpa}$
$v=0.27$	$\rho=1700\,\mathrm{kg/\,m^3}$	$layups[0^\circ,90^\circ]$	

By substituting displacement fields in the potential and kinetic energies and applying the standard procedure, the mass and stiffness matrices of the element can be obtained which are presented in the Appendix.

By discretizing the whole beam into n elements, the total displacement vector, q, has $6n+3$ degrees of freedom. After assembling the global mass and stiffness matrices, [M] and [K], respectively, the equations of motion can be represented as follows:

$$[M]\{\ddot{q}\}+[K]\{q\}=\{f\} \tag{26}$$

In this equation, the dot shows derivation with respect to time, so it is obvious that $\{\ddot{q}\}$ shows the acceleration vector. In addition, $\{f\}$ indicates the total force vector. Since there is only a concentrated force in the radial direction, the values of the force vector have been obtained based on the force location, i.e., if the point force F_0 is located on the ith element, the values of the force vector are obtained as:

$$\begin{aligned}(3(2i-1)-1)&=N_1(\xi)F_0\\(3(2i-1)+2)&=N_2(\xi)F_0\\(3(2i-1)+5)&=N_3(\xi)F_0\end{aligned} \tag{27}$$

In which ξ indicates the local position of the point force. Eq. (26) shows the coupled linear differential equations. The Newmark method in this section is employed to solve Eq. (26). If $\{q_n\}$ shows the displacement vector at the nth time step, using the Newmark method, $\{q_{n+1}\}$ can be obtained as follows [10]:

$$\begin{aligned}\{q\}_{n+1}&=\{q\}_n+\Delta t\{q\}+(0.5-\alpha)\{q\}_n+\alpha\Delta t^2\{\ddot{q}\}_{n+1}\\\{\dot{q}\}_{n+1}&=\{\dot{q}\}_n+(1-\beta)\Delta t\{q\}_n+\beta\Delta t\{q\}_{n+1}\end{aligned} \tag{28}$$

Δt is defined as $t_{n+1}-t_n$. It should be mentioned that the coefficients α, β are 0.5 and 0.7, respectively [10]. substituting Eq. (28) into Eq. (26) yields the following matrix form:

$$\left[\hat{K}\right]\{q\}_{n+1}=\left[\hat{F}\right]_{n+1} \tag{29}$$

In which the modified stiffness matrix $\left[\hat{K}\right]$ and force vector $\left[\hat{F}\right]$ for each time step can be calculated as:

By solving the algebraic Eq. (29), the dynamic response can be obtained.

$$\begin{aligned}\left[\hat{K}\right]&=[K]+\frac{1}{\alpha\Delta t^2}[M]\\\left[\hat{F}\right]_{n+1}&=\{F\}_{n+1}+[M]\frac{1}{\alpha\Delta t^2}(\{q\}_n+(0.5-\alpha)\Delta t^2\{q\}_n)\end{aligned} \tag{30}$$

4- Validation

To validate the results, we have compared free and forced vibrational results with available literature and ANSYS software. Unless mentioned otherwise, the physical and geometrical properties of the beam are listed in Table 1. In the first part, we compared natural frequencies. According to Table 2, the fundamental frequency of the present st-udy has been compared with Refs. [20] and [27]. Two types of boundary conditions, i.e., simple-simple (S-S) and clamped-clamped (C-C), are considered. As can be observed, there are good agreements between our results and previous studies. The maximum difference of 1.208 percent has been seen.

In order to compare higher mode frequencies, we have modeled a 3D composite curved beam in ANSYS software. Solid46 element in ANSYS is employed to simulate the beam and also C-C boundary conditions have been considered. In Table 3, the first five dimensionless frequencies are compared with ANSYS and Ref. [20]. Very good agreements have been observed.

In the second part, forced vibrational results against the ANSYS model are compared. In this case, a harmonic downward nonmoving force, i.e., $f=-1000\sin(300t)N$, in the middle of the beam is assumed. Fig. 3, shows the radial displacement of the middle point versus time. As can be clearly observed in Fig. 3, the results are in good agreement with ANSYS, especially in the early time of the simulation.

Table 2. Dimensionless fundamental frequency parameter ($\Omega = \omega R^2 \theta_0^2 \sqrt{12\rho / E_{11} h^2}$)

	s-s			c-c	
$\frac{E_{11}}{E_{22}} = 15$	Present	[27] (Percentage of difference)	[20] (Percentage of difference)	Present	[20] (Percentage of difference)
$\frac{h}{R} = 0.05$	14.905	14.880 (0.167%)	14.891 (0.093%)	24.680	24.681 (0.004%)
$\frac{h}{R} = 0.1$	14.977	14.964 (0.086%)	14.976 (0.006%)	23.617	23.490 (0.537%)
$\frac{h}{R} = 0.15$	14.834	14.768 (0.444%)	14.779 (0.370%)	21.920	21.655 (1.208%)

Table 3. First five dimensionless frequencies ($\Omega = \omega R^2 \theta_0^2 \sqrt{12\rho / E_{11} h^2}$)

Mode number	Present	ANSYS	[20]
1	24.680	23.944	24.681
2	48.25	46.89	48.19
3	86.628	84.316	86.386
4	124.452	122.07	123.93
5	177.706	168.239	176.62

Table 4.

$E_{11} = 144.8$ Gpa	$G_{13} = 5.5$ Gpa	$\rho = 1389.297$ kg/m^3
$E_{22} = 9.65$ Gpa	$\nu = 0.25$	

5- Numerical Results and Discussion

Parametric studies for laminated composite curved beams are presented to investigate the effects of different parameters such as boundary conditions, total angle of the beam, and fiber orientations on the vibrational characteristics of the beam. Also, the resonance phenomenon for different boundary conditions is discussed. Convergence study of results for a different number of elements i.e., 10, 50, and 100 elements, have been examined and shown in Fig. 4. As can be seen in Fig. 4, there is good agreement between results by considering 50 elements. Thus, to calculate our results, we consider 50 elements that provide good accuracy. It should be mentioned that number of time steps in this method are considered to be $1000-5000$ for different cases to obtain convergent results. In this section, the physical and geometrical properties of the beam are listed in Table 4.

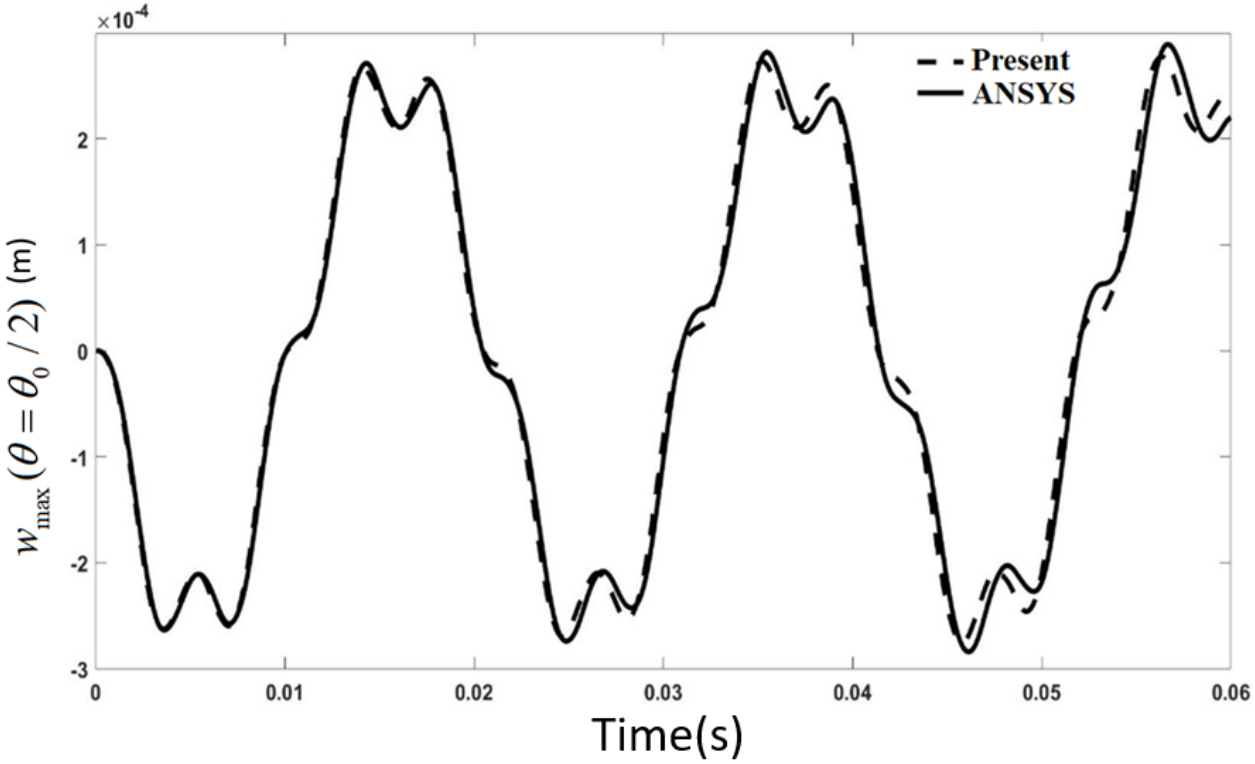

Fig. 3. Validation of transient response for a curved beam under harmonic load

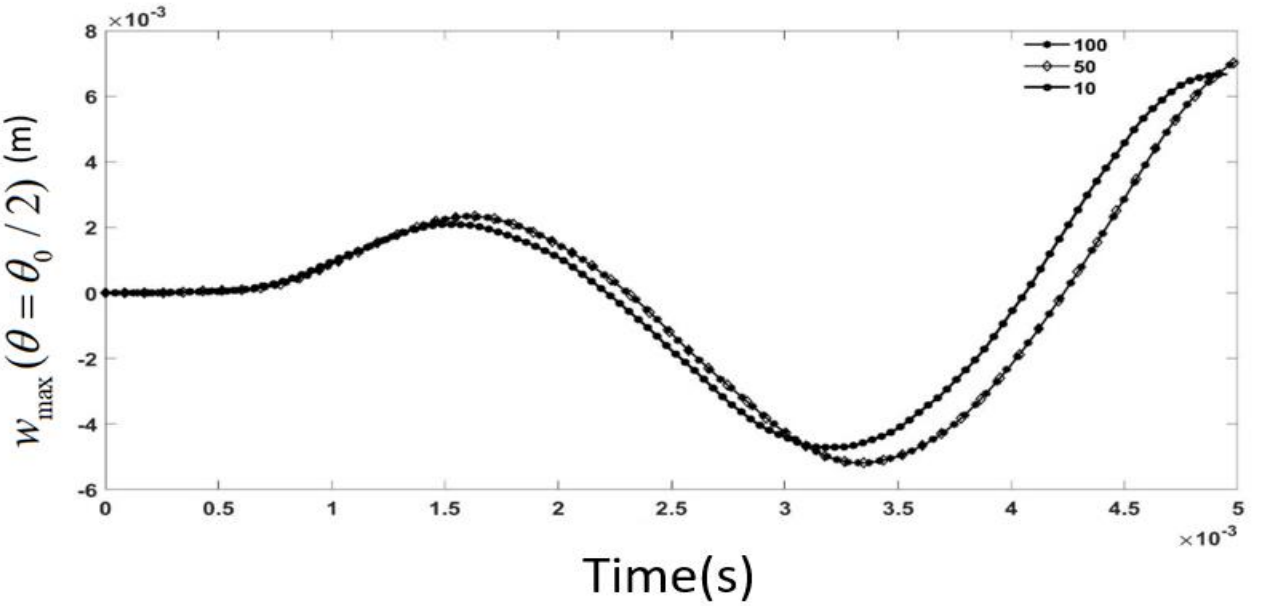

Fig. 4. Effect of the number of elements on the transient response

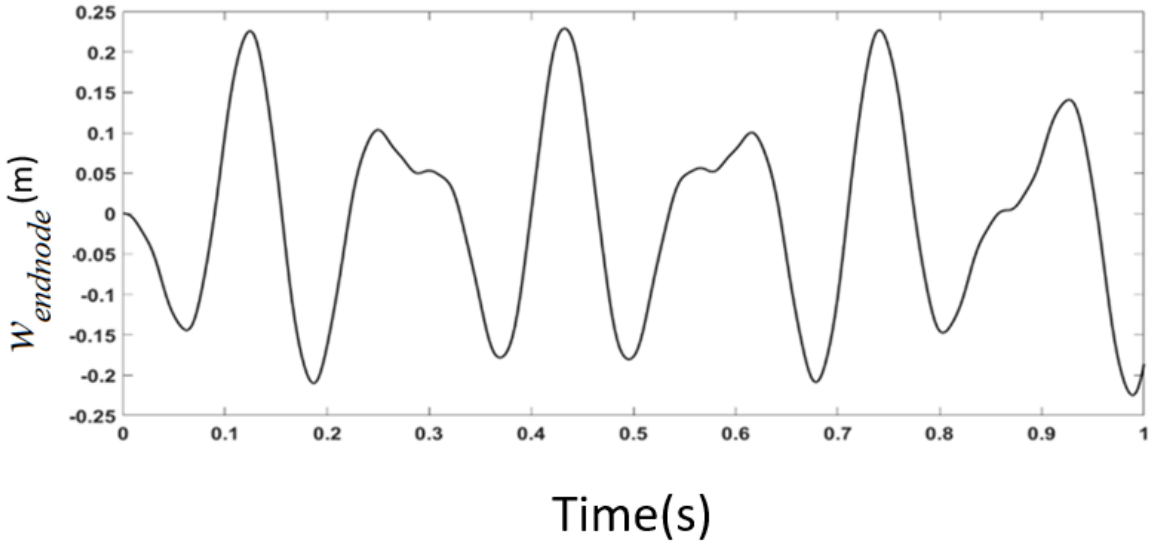

(a)

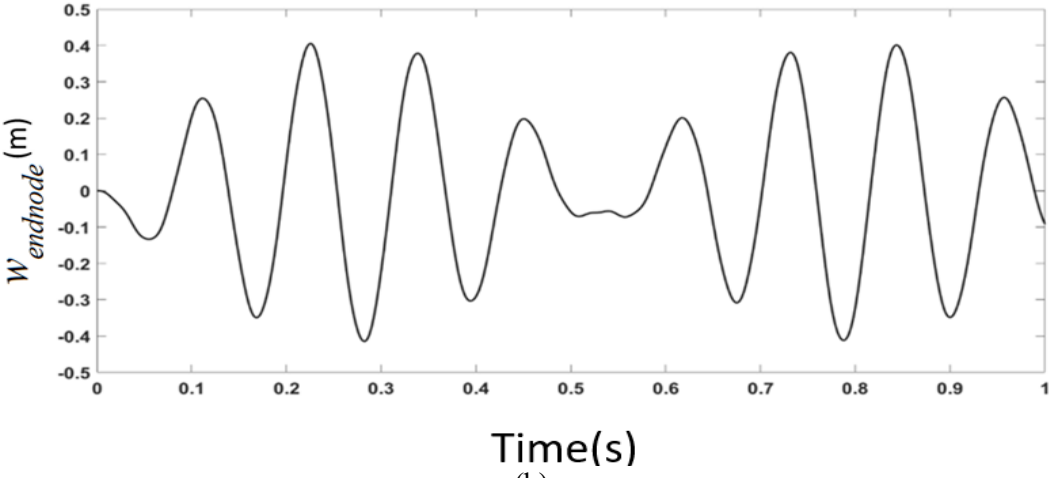

(b)

Fig. 5. Dynamic response of the free end of the beam under harmonic load for different excitation frequencies ($L = 1$ m, $\theta_0 = 2\pi / 3$ rad) (a: $\omega = 40$ rad/sec, b: $\omega = 50$ rad/sec

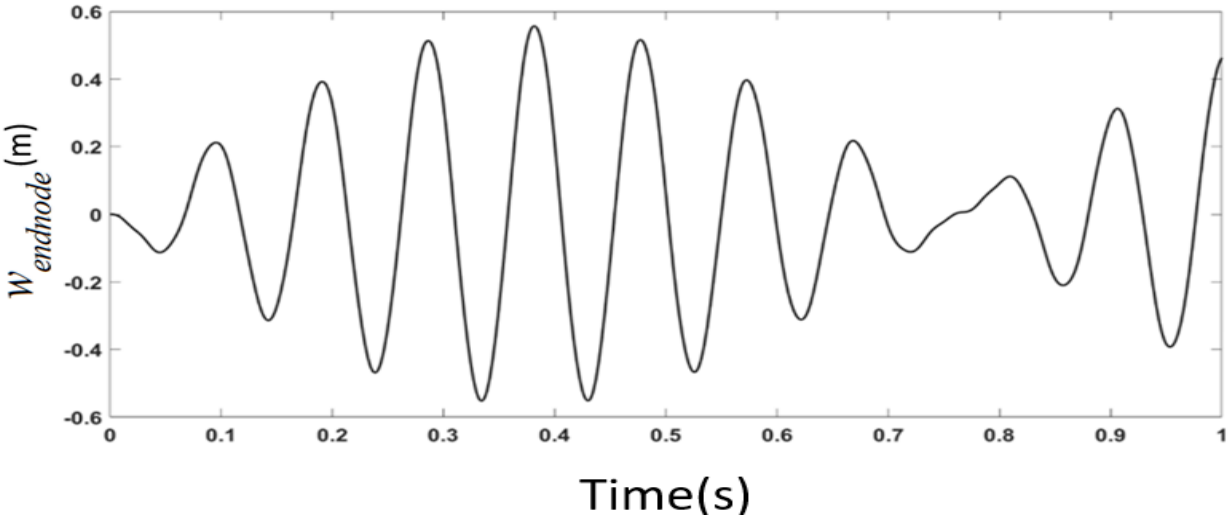

(c)

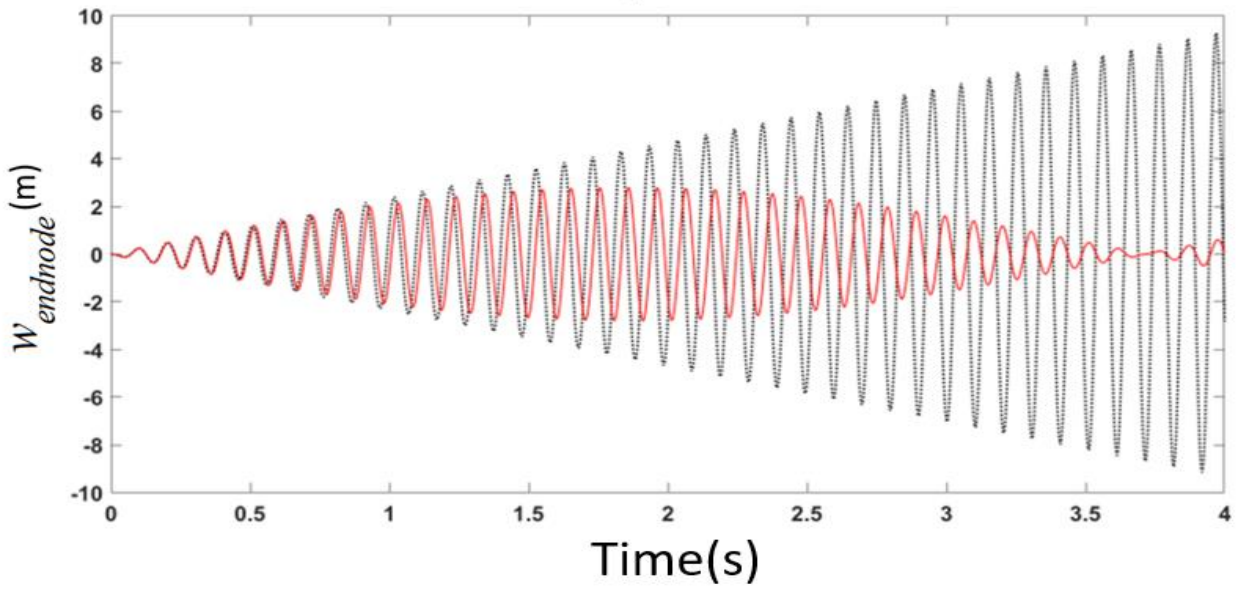

(d)

Fig. 5. Dynamic response of the free end of the beam under harmonic load for different excitation frequency ($L = 1$ m, $\theta_0 = 2\pi / 3$ rad)(c: $\omega = 70$ rad/sec, d: $\omega = 60$ rad/sec (solid line), ($\omega = 61.7984$ rad/sec dot line))

Table 5. First five dimensionless frequencies ($\Omega = \omega R^2 \theta_0^2 \sqrt{12\rho / E_{11} h^2}$)

Mode number	C-C	S-S
1	24.509	14.827
2	47.786	37.350
3	85.487	70.170
4	122.336	109.221
5	173.804	155.690

5- 1- Effect of harmonic excitation

In this section, the effect of harmonic load, $f = -1000\sin(\omega t)\ N$, on the dynamic response of the clamped-free laminated composite beam has been studied. The nonmoving force is located at the free end of the beam and the deflection of the endpoint of the beam versus time is plotted in Fig. 5. As can be seen when the excitation frequency is getting close to the fundamental frequency of the beam, the beam is prone to experience a resonance phenomenon. However, the beam experience resonance is just for the excitation frequency exactly equal to the fundamental frequency ($\omega = \omega_n = 61.7984$ rad/sec), (Fig. 5(d)). Moreover, in Fig. 5(d), we can see that the beating phenomena occur when the excitation frequency ($\omega = 60$ rad/sec) is very close to the fundamental frequency.

5- 2- Effect of boundary conditions

Table 5 shows the effect of boundary conditions on the natural frequencies. As it is expected, it can be observed that the clamped-clamped beam has the highest value for natural frequencies and the minimum value has been observed for the simple-simple boundary condition.

The corresponding mode shapes of the laminated composite curved beam have been depicted in Fig. 6.

5- 3- Transient response of the curved beam subjected to the moving force

In this section, parametric studies have been done to investigate different parameters on the transient response of the laminated composite curved beam. Unless mentioned otherwise, the radius and total angle of the beam are taken to be 0.5 m and $\pi / 2$ rad, respectively.

5- 3- 1- The effect of boundary conditions

Fig. 7 shows the maximum deflection i.e., w at the beam center vs dimensionless velocity (T_f / τ). τ denotes the fundamental period of the beam and T_f is the time duration that force exists on the beam and can be expressed

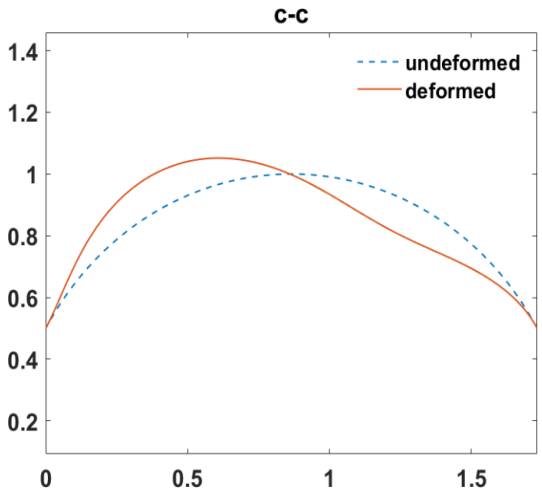

(a) First mode shape

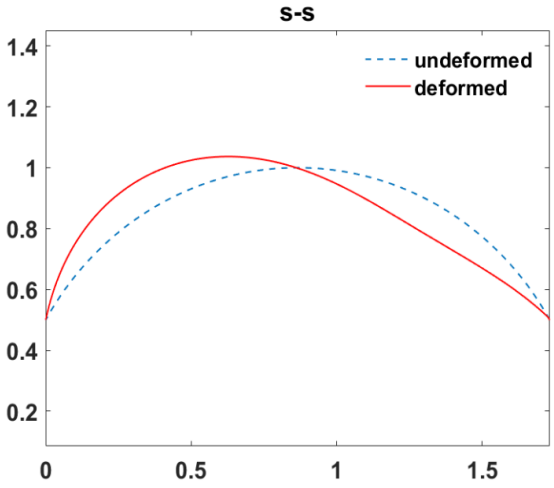

(b) First mode shape

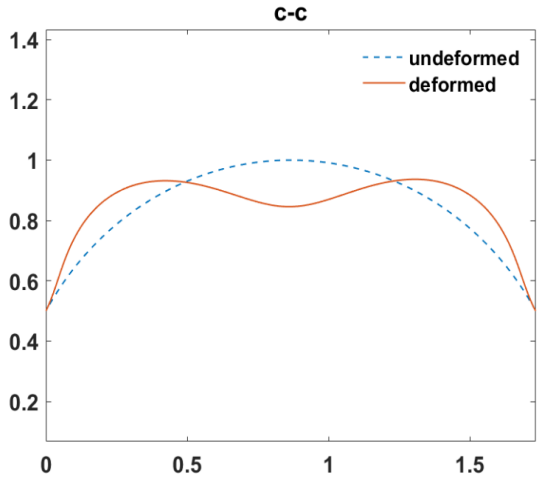

(c) Second mode shape

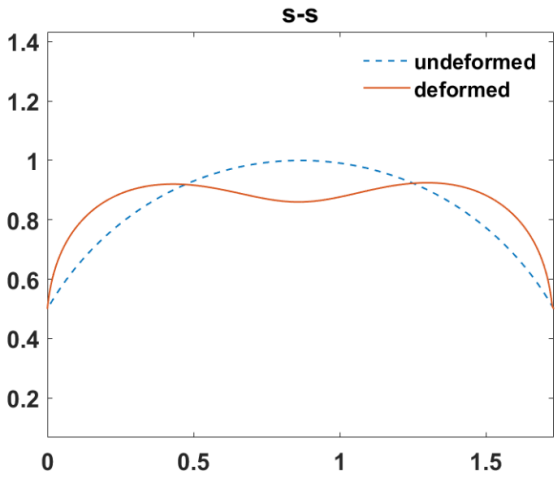

(d) Second mode shape

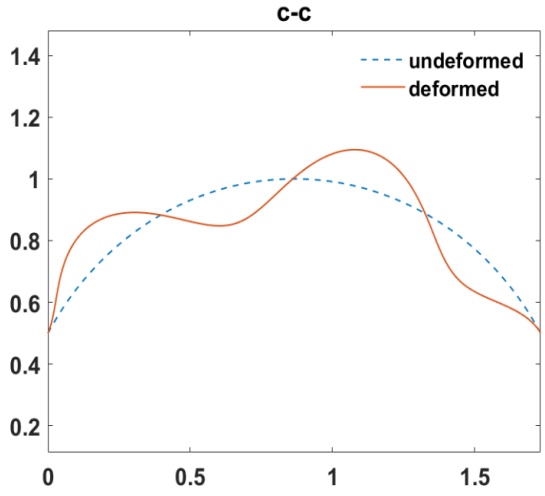

(e) Third mode shape

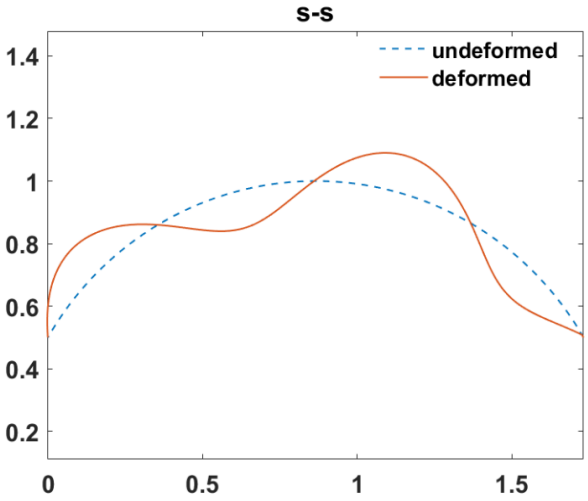

(f) third mode shape

Fig. 6. First four mode shapes of the beam for C-C and S-S boundary conditions (continued on the next page)

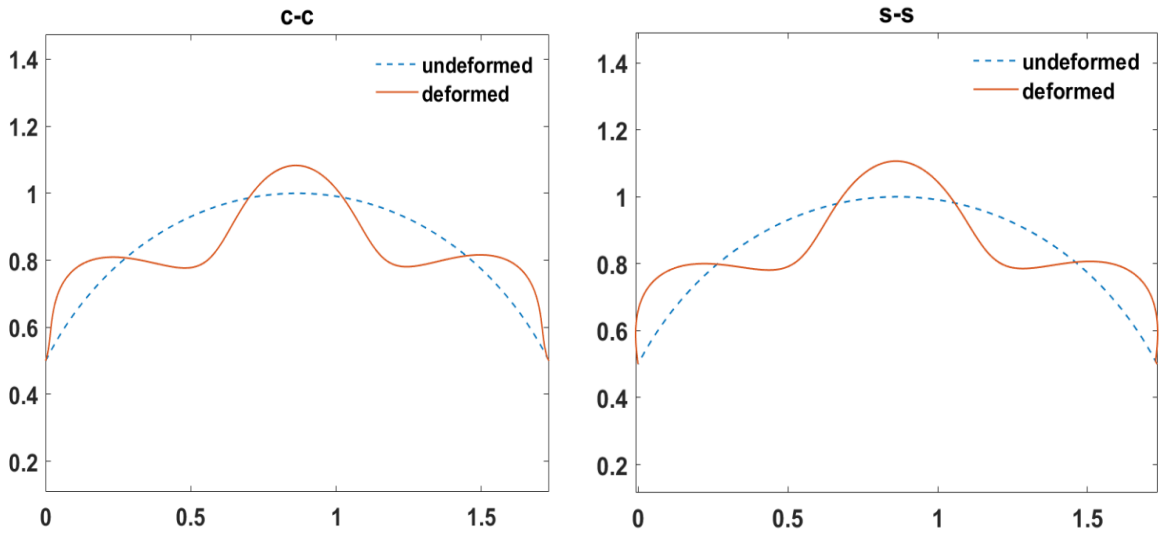

(g) Fourth mode shape (h) Fourth mode shape

Fig. 6. First four mode shapes of the beam for C-C and S-S boundary conditions. (continued from the previous page)

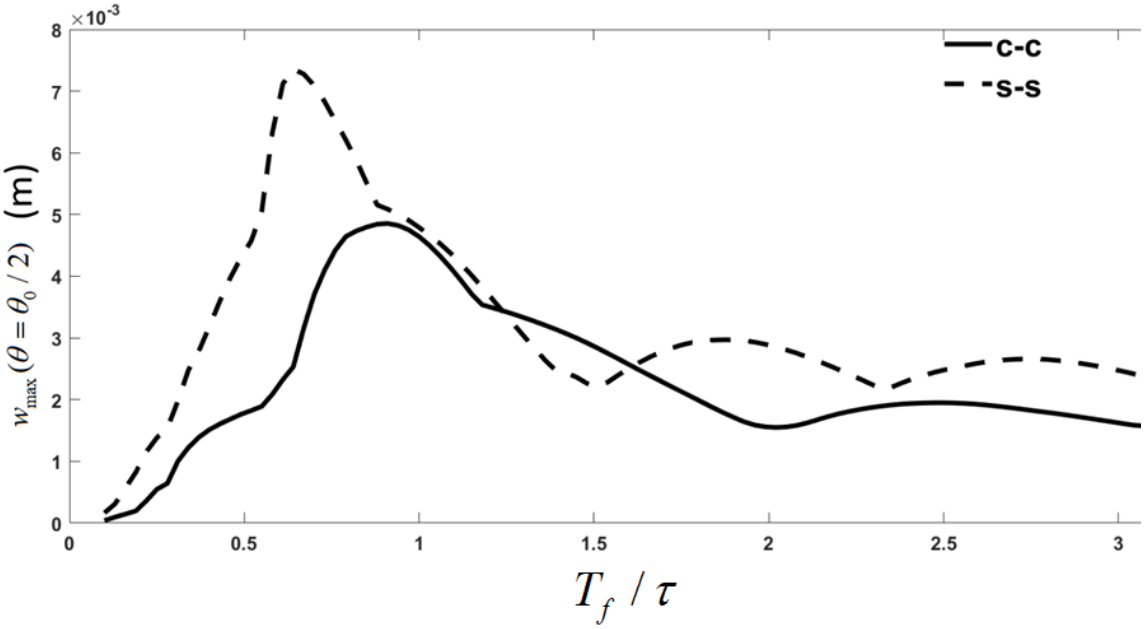

Fig. 7. Variation of w_{max} vs. T_f/τ for two layered beams ($[0^\circ,90^\circ]$) with C-C and S-S boundary conditions

as ($T_f=\frac{l}{v}$). As can be seen from Fig. 7, w_{max} has an insignificant value in lower dimensionless velocity. This is likely to happen due to the fact that there is not enough time for the occurrence of the beam deflection when the velocity of moving force is high i.e., low value of $\frac{l}{v}$. It should be mentioned that the laminated composite curved beam with clamped-clamped boundary condition represented greater stiffness than the simple-simple one, and due to this reason, it has a lower deflection which can be obviously seen in most parts of Fig. 7.

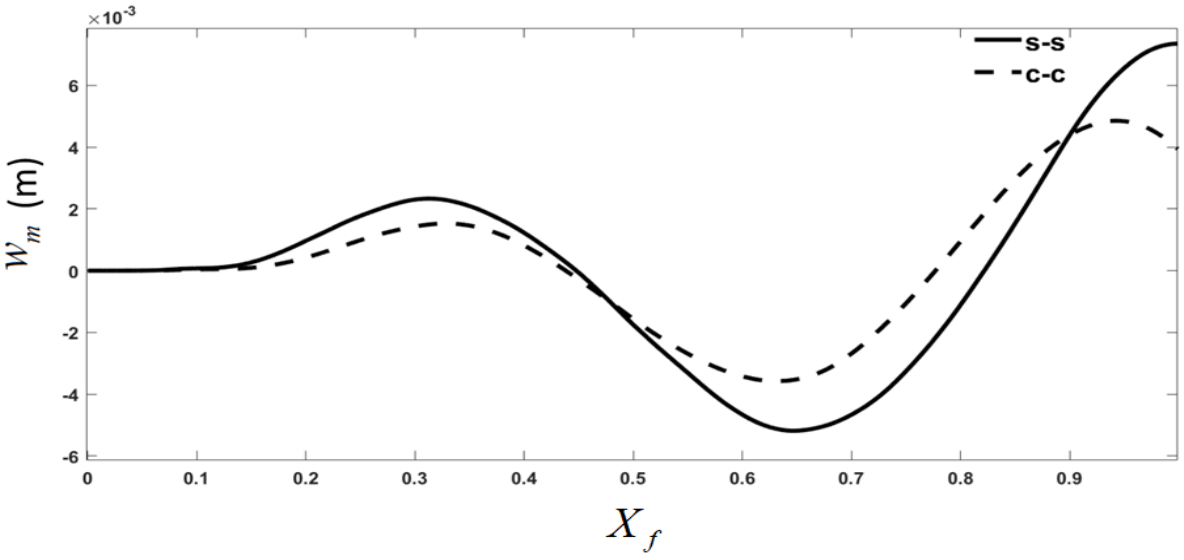

Fig. 8. Variation of deflection at the beam center (w_m) vs. at critical load velocity for two layered beams ($[0^\circ, 90^\circ]$)

Referring to Fig. 7, critical dimensionless velocity can be defined as the velocity when the maximum deflection occurs at the beam center. This critical dimensionless velocity is obtained at 0.91 and 0.64 for C-C and S-S boundary conditions, respectively. It can be concluded that the critical velocity in the C-C boundary conditions is close to the first period of the beam. In Fig. 8, the deflection of the beam center w_m versus dimensionless point force position (X_f) is shown in its critical velocity. $X_f = 0$ indicates that the force is on the left end of the beam and $X_f = 1$ indicates that the force is on the right end of the beam. It can be seen that, the maximum value for w_m occurs when the load is in the verge of leaving the beam. It should be noted that, simple end conditions for laminated composite curved beam, provides more deflections compared to the clamped end conditions.

5- 3- 2- Effect of total angle of the beam

The transient response of the beam for the constant value of the beam's length ($L = R\theta_0$) is calculated by assuming different values for a total angle of the beam (θ_0). Fig9 . (a) and (b), show the maximum deflection of the beam center for two different boundary conditions, i.e., clamped-clamped and simple-simple. It can be observed that in a simply supported beam, increasing the total angle (θ_0), causes the vertical deflection to increase. Moreover, maximum deflection for simply supported beam occurs in lower load velocity for higher values of total angle. Also, for clamped-clamped boundary conditions, the same behavior can be seen except for $\theta_0 = \frac{\pi}{6}$ rad. In general, the beam under the action of moving force with high velocity has the lowest deflection for a different total angles of the beam. This can be due to the fact that the beam doesn't have enough time to respond to the movement of the force.

5- 3- 3- Effect of fiber orientations

In this section, the effect of fiber orientation on the dynamic response of the beam with cross-ply and angle-ply lamination schemes is investigated. Results have been presented for four-layered simply supported beams. The other parameters are the same as the previous sections. Different stacking sequences have been considered namely $[0^\circ, 90^\circ, 0^\circ, 90^\circ]$ and $[0^\circ, 90^\circ, 90^\circ, 0^\circ]$ for symmetric and anti-symmetric cross-ply layups, respectively, and angle-ply layups $[\theta, -\theta, \theta, -\theta]$. As can be seen from Fig. 10(a), the maximum deflection response for the case of symmetric cross-ply is smaller than that of the anti-symmetric one. Moreover, it is seen from Fig. 10(b) that increasing the angle of fiber orientation in angle-ply layups causes the dynamic response of the beam to increase. The reason is that increasing the angle of fiber orientation decreases the bending stiffness of the beam. In addition, as can be observed in Fig. 10(b), differences between the transient response for $\theta = 60^\circ$ and $\theta = 90^\circ$ are insignificant which is due to the fact that the difference between their bending stiffness is small. The most notable differences between different fiber orientations can be observed between cross-ply and angle-ply laminates. By comparing these two figures, it is evident that the cross-ply laminates have more stiffness than the angle-ply laminates. In other words, it shows that choosing different fiber orientations can influence the stiffness of the structure and so different response will be obtained.

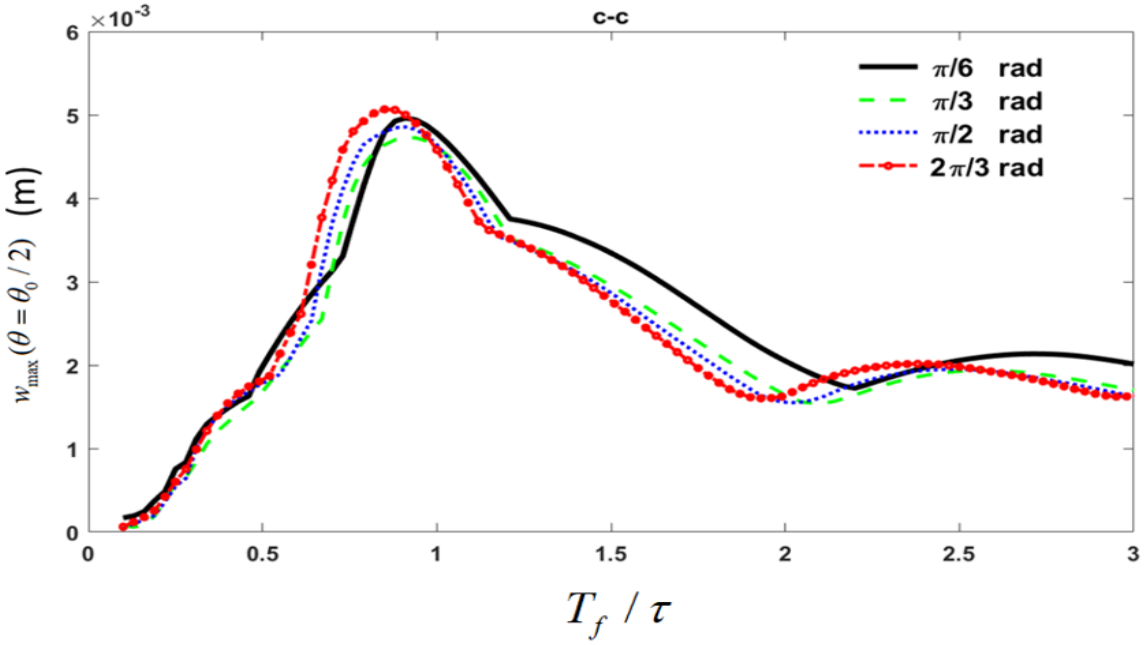

(a)

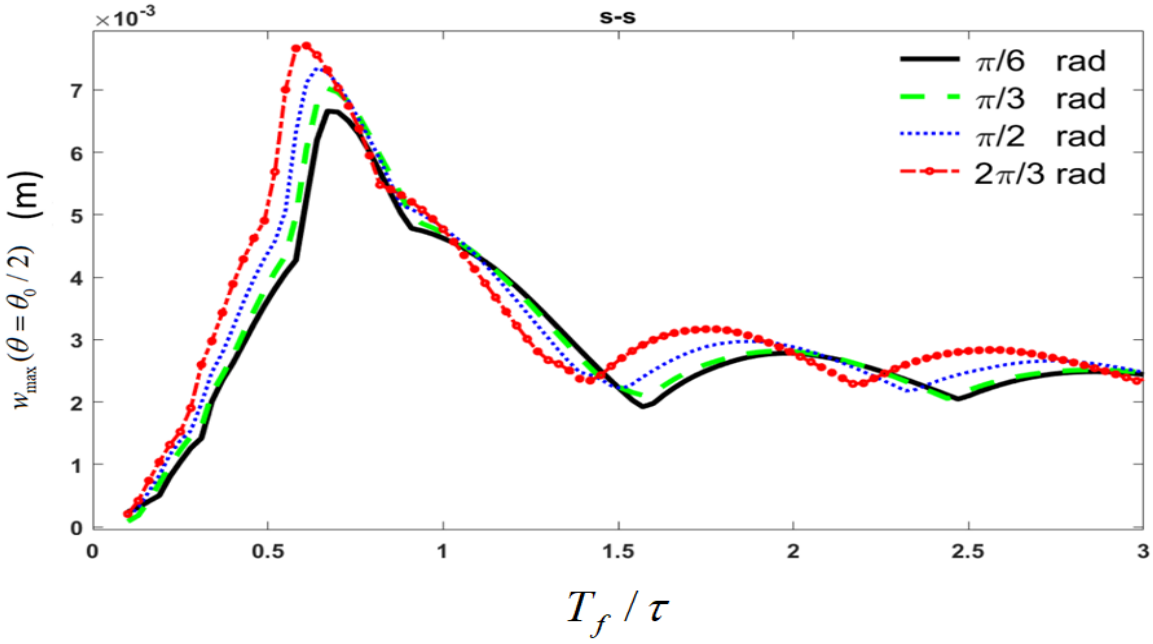

(b)

Fig. 9. Variation of w_{max} vs. T_f / τ for a different total angles of the two-layered beams ($[0^\circ, 90^\circ]$).(a: clamped-clamped; b: simple-simple)

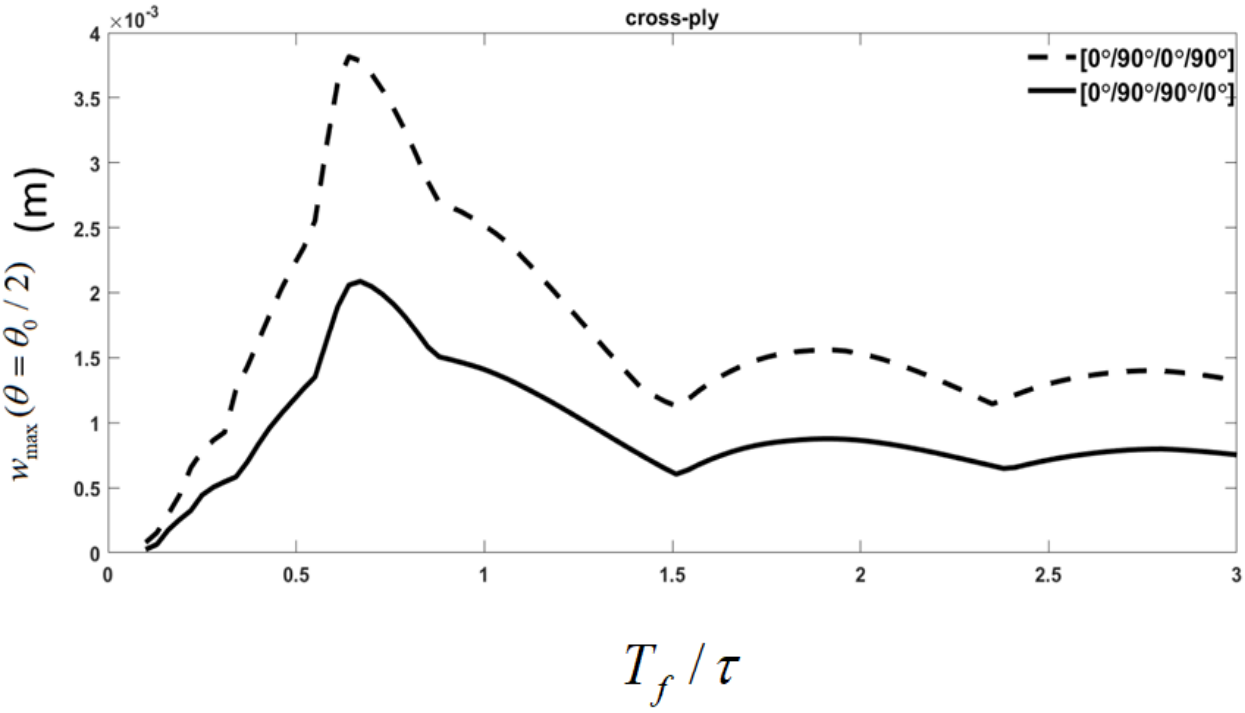

(a)

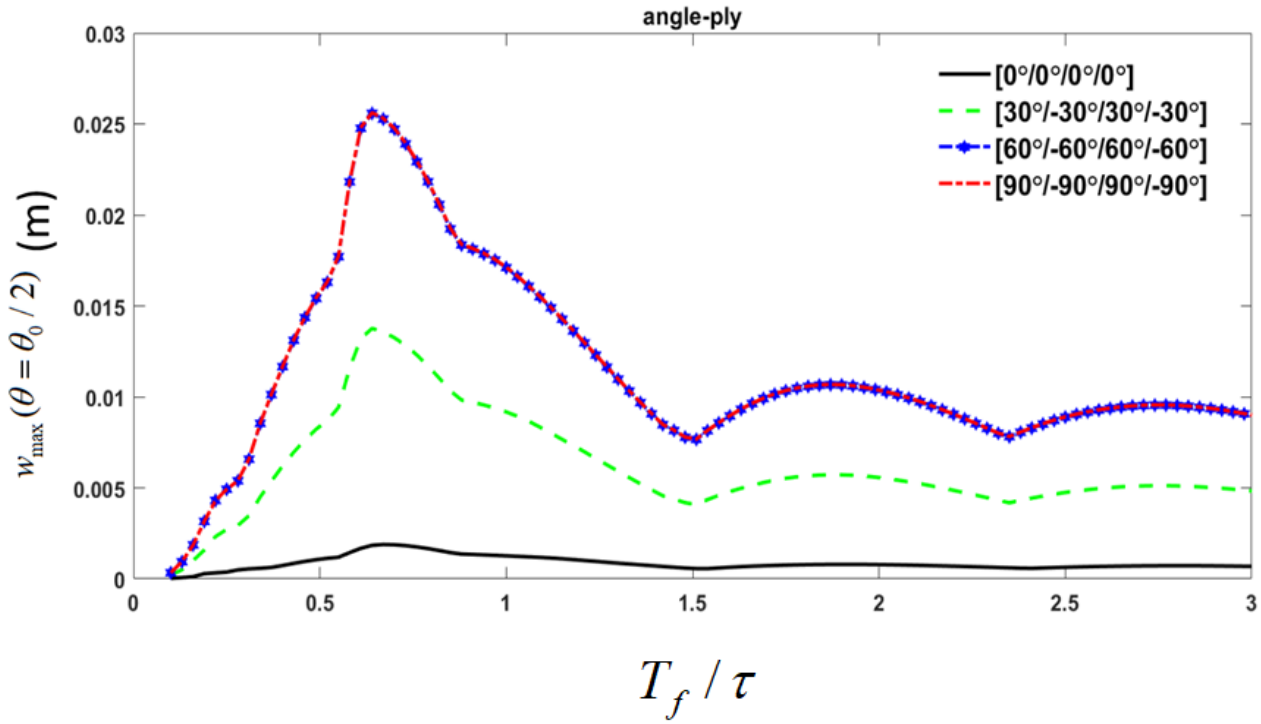

(b)

Fig. 10. Variation of w_{max} of the beam center vs. T_f/τ for cross-ply and angle-ply stacking sequences.(a: cross-ply) (b: angle-ply)

6- Conclusion

Free and forced vibration analysis of the laminated curved beams is presented in this study. The effects of shear deformation, rotary inertia, and material coupling are taken into account. The finite element method is used to solve the governing equations of motion. The obtained natural frequencies are validated by comparing the present results against available results in the literature and ANSYS. Likewise, the results of forced vibration analysis of the curved beam are verified against ANSYS. The effects of different parameters on the vibrational characteristics and also the transient response of the beam have been investigated in detail. Based on the numerical results, the boundary conditions have a significant influence on the response of the laminated composite curved beam. It is shown that the beam with clamped–clamped ends has the lowest transient deflection and highest frequency which is due to the highest overall stiffness of this kind of boundary condition. Likewise, it is found that the clamped-clamped beam has a higher critical velocity with respect to the beam with simple-simple end conditions.

The inspection released that the beam with cross-ply layups has lower values of transient deflection compared to the angle-ply layups. Moreover, the anti-symmetric cross-ply beam has more deflection in comparison with the symmetric one. Likewise, it is shown that by increasing the angle of fiber orientation in angle-ply layups, the dynamic response of the beam increases.

Appendix

Element mass and stiffness matrices

For each element, the mass and stiffness matrices are calculated as follows:

$$[M]^e = R\theta_0 \int_0^1 (\overline{I}_0^e [N_u]^T [N_u] + \overline{I}_1^e [N_u]^T [N_\psi] + \overline{I}_2^e [N_\psi]^T [N_\psi] + \overline{I}_0^e [N_w]^T [N_w]) d\zeta \quad \text{(A.1)}$$

$$\begin{aligned}[K]^e = \int_0^1 [&\frac{A_{11}}{R\theta_0}[N_{u,\theta}]^T [N_{u,\theta}] + \frac{A_{11}\theta_0}{R}[N_w]^T [N_w] + \frac{A_{11}}{R}[N_{u,\theta}]^T [N_w] \\ &+ \frac{A_{11}}{R}[N_w]^T [N_{u,\theta}] + \frac{B_{11}}{R\theta_0}[N_{\psi,\theta}]^T [N_{u,\theta}] \\ &+ \frac{B_{11}}{R\theta_0}[N_{u,\theta}]^T [N_{\psi,\theta}] + \frac{B_{11}}{R}[N_{\psi,\theta}]^T [N_w] + \frac{B_{11}}{R}[N_w]^T [N_{\psi,\theta}] + \\ &\frac{D_{11}}{R\theta_0}[N_{\psi,\theta}]^T [N_{\psi,\theta}] + \frac{A_{55}}{R\theta_0}[N_w]^T [N_w] \\ &+ \frac{A_{55}\theta_0}{R}[N_{u,\theta}]^T [N_{u,\theta}] + A_{55}\theta_0 R[N_{\psi,\theta}]^T [N_{\psi,\theta}] \\ &- \frac{A_{55}}{R}[N_{w,\theta}]^T [N_u] - \frac{A_{55}}{R}[N_u]^T [N_{w,\theta}] \\ &- A_{55}R[N_{w,\theta}]^T [N_\psi] - A_{55}R[N_\psi]^T [N_{w,\theta}] \\ &- A_{55}\theta_0 [N_u]^T [N_\psi] - A_{55}\theta_0 [N_\psi]^T [N_u]] d\zeta \end{aligned} \quad \text{(A.2)}$$

References

[1] Report of the Commissioners Appointed to Inquire Into the Application of Iron to Railway Structures, William Clowes and sons, (1) (1849).

[2] Y. Dugush , M. Eisenberger, Vibrations of non-uniform continuous beams under moving loads, Journal of Sound and vibration, 254(5) (2002) 911-926.

[3] G. Stokes, Discussion of a differential equation relating to the breaking of railway bridges, Printed at the Pitt Press by John W. Parker, (1849)

[4] S.Timoshenko, On the transverse vibrations of bars of uniform cross-section, The London, Edinburgh, and Dublin Philosophical Magazine and Journal of Science, 43(253) (1922) 125-131.

[5] Y.B. Yang, J.D. Yau, Y.S Wu, Vehicle-bridge interaction dynamics: with applications to high-speed railways, World Scientific, (2004).

[6] B. Gören Kiral, Z. Kiral, B. Okutan Baba, Dynamic behavior of laminated composite beams subjected to a moving load, Journal of Applied Sciences, 4(2) (2004) 271-276.

[7] V. Kahya, Dynamic analysis of laminated composite beams under moving loads using finite element method, Nuclear engineering and design, 243 (2012) 41-48.

[8] M.H. Kargarnovin , R.A. Jafari-Talookolaei, M.T. Ahmadian, Vibration analysis of delaminated Timoshenko beams under the motion of a constant amplitude point force traveling with uniform velocity, International Journal of Mechanical Sciences, 70 (2013) 39-49.

[9] M.H. Kadivar, S.R. Mohebpour, Finite element dynamic analysis of unsymmetric composite laminated beams with shear effect and rotary inertia under the action of moving loads, Finite elements in Analysis and Design, 29(3-4) (1998) 259-273.

[10] R.A. Jafari-Talookolaei, M.H. Kargarnovin, M.T. Ahmadian, Dynamic response of a delaminated composite beam with general lay-ups based on the first-order shear deformation theory, Composites Part B: Engineering, 55 (2013) 65-78.

[11] V. Kahya, A. Mosallam, Dynamic analysis of composite sandwich beams under moving mass, Kahramanmaraş Sütçü İmam Üniversitesi Mühendislik Bilimleri Dergisi, 14(1)(2011).

[12] H. Zibdeh, M. Abu-Hilal, Stochastic vibration of laminated composite coated beam traversed by a random moving load, Engineering structures, 25(3) (2003) 397-404.

[13] J. Genin, E.C. Ting, Z. Vafa, Curved bridge response to a moving vehicle, Journal of Sound and Vibration, 81(4) (1982) 469-475.

[14] Y.B. Yang, C.M. Wu, J.D. Yau, Dynamic response of a horizontally curved beam subjected to vertical and horizontal moving loads, Journal of Sound and vibration, 242(3) (2001) 519-537.

[15] J.S. Wu, L.K. Chiang, Out-of-plane responses of a circular curved Timoshenko beam due to a moving load, International Journal of Solids and Structures, 40(26) (2003) 7425-7448.

[16] S.H. Li, J.Y. Ren, Analytical study on dynamic responses of a curved beam subjected to three-directional moving loads, Applied Mathematical Modelling, 58 (2018) 365-387.

[17] M. Arefi, A.M. Zenkour, Transient sinusoidal shear deformation formulation of a size-dependent three-layer piezo-magnetic curved nanobeam, Acta Mechanica, 228(10) (2017) 3657-3674.

[18] M. Arefi, E. Mohammad-Rezaei Bidgoli, R. Dimitri, M. Bacciocchi, F. Tornabene, Nonlocal bending analysis of curved nanobeams reinforced by graphene nanoplatelets, Composites Part B: Engineering, 166 (2019)1-12.

[19] M. Hajianmaleki, M.S. Qatu, Static and vibration analyses of thick, generally laminated deep curved beams with different boundary conditions, Composites Part B: Engineering, 43(4) (2012) 1767-1775.

[20] T. Ye, G. Jin, X. Ye, X. Wang, A series solution for the vibrations of composite laminated deep curved beams with general boundaries, Composite Structures, 127 (2015) 450-465.

[21] R.A. Jafari-Talookolaei, M. Abedi, M. Hajianmaleki, Vibration characteristics of generally laminated composite curved beams with single through-the-width delamination, Composite Structures, 138 (2016) 172-183.

[22] X.X. Qin, H.P. Chen, S.J. Wang, Analytical Solution of Composite Curved I-Beam considering Tangential Slip under Uniform Distributed Load, Mathematical Problems in Engineering,2021 (2021)4094753.

[23] J. Luo, S. Zhu, W. Zhai, Formulation of curved beam vibrations and its extended application to train-track spatial interactions, Mechanical Systems and Signal Processing, 165 (2022)108393.

[24] D. Shao, S. Hu, Q.Wang, F. Pang, A unified analysis for the transient response of composite laminated curved beam with arbitrary lamination schemes and general boundary restraints, Composite Structures, 154 (2016) 507-526.

[25] H. Kurtaran, Geometrically nonlinear transient analysis of thick deep composite curved beams with generalized differential quadrature method, Composite Structures, 128 (2015) 241-250.

[26] J. Zhao, Z. Gao, H. Li, J. Guan, Q. Han, Q. Wang, A unified modeling method for dynamic analysis of CFRC-PGPC circular arche with general boundary conditions in hygrothermal environment, Composite Structures, 255 (2021) 112884.

[27] H. Sarparast, A. Ebrahimi-Mamaghani. Vibrations of laminated deep curved beams under moving loads, Composite Structures, 226 (2019) 111262.

HOW TO CITE THIS ARTICLE
A. Ahmadi, M. Abedi, Transient Response of Laminated Composite Curved Beams with General Boundary Conditions under Moving Force, AUT J. Mech Eng., 6(4) (2022) 561-578.

DOI: 10.22060/ajme.2022.20787.6020